Aberystwyth University

Micro-mechanical prediction of the effect of surfactant concentration and external friction on the visco-elasto-plastic response of an aqueous foam
Zaccagnino, Francesca; Cox, Simon

Journal Name

Micro-mechanical prediction of the effect of surfactant concentration and external friction on the visco-elasto-plastic response of an aqueous foam

Francesca Zaccagnino[a] and Simon Cox[b]

We apply a combination of the Viscous Froth model and a surfactant transfer model [Zaccagnino *et al., Phys. Rev. E*, 2018, **98**, 022801] to predict the rheological response of a two-dimensional dry aqueous foam. The model includes both the effect of friction between the foam and the boundaries of the container and also the dissipative effects on the film interfaces caused by surfactant motion. These dynamics are characterized by two free parameters: the Gibbs elasticity, relating surfactant concentration to interfacial tension, and the mobility of the surfactant molecules on the interfaces. We employ numerical simulations to evaluate the static shear modulus, yield stress and the storage and loss moduli of a foam and investigate the effect of our free parameters on these rheological properties.

1 Introduction

Soft glassy materials such as emulsions, microgels, granular materials, colloidal suspensions and aqueous foams, when subjected to shear strain at constant shear rate, present a similar stress response. They are called yield stress materials and are characterized by a variation from a solid-like behaviour, at low shear stress, to a liquid-like one when the applied stress is higher than a critical value[1]. The yield stress confers on these materials remarkably useful properties: when the stress increases beyond the yield value the foam flows like a viscous non-Newtonian fluid. By carefully controlling the yield stress, for example, mayonnaise is easy to spread and yet it doesn't run[2]. Rheological properties are important for applications in several fields, from the food sector to the medical industry in which, for example, endovenous microfoams are used to treat varicose veins[3].

In an aqueous foam, the microstructure (bubbles, soap films)

---
[a] *Department of Mathematics, Aberystwyth University, Wales, UK; E-mail: frz@aber.ac.uk*
[b] *Department of Mathematics, Aberystwyth University, Wales, UK; E-mail: sxc@aber.ac.uk*

tends to be visible and foams therefore provide a valuable material for validating predictions at this level[4,5]. In the present work we consider dry foams, which are foams characterized by low liquid fraction, ϕ_l. The dry limit, defined by $\phi_l < 5\%$[4], is the condition present when the amount of liquid at film intersections is less than 5%. At low liquid fraction, foams are typical visco-elasto-plastic materials, and the yield stress and the shear modulus are the appropriate parameters to characterize their rheological properties[4,6].

Predictions of the elastic response of foam were pioneered by Princen, with a model of a hexagonal 2D foam[7]. Kruyt[8] predicted the effect of disorder on the shear modulus, while Stamenovic[9] gave a prediction for ordered dry 3D foams.

Simulations using Brakke's Surface Evolver[10] provide a means to validate such predictions at the bubble scale for ordered[11] and disordered 2D[12] and 3D[13] dry foams. Experimental data confirms that the shear modulus decreases with increasing liquid content and is inversely proportional to the bubble size[14]. Predicting the effects of strain-rate on the shear modulus is more difficult.

Furthermore, even in the dry limit, there are few detailed stud-

ies of the yield stress of a foam[6,7] and measurements of complex shear moduli[15–18].

Experimentally, the response of a foam flowing at constant shear rate is well described by the Herschel-Bulkley constitutive equation[19,20], although there is no consensus on how the free parameters of the constitutive law (for example the consistency and shear-rate exponent) depend on the geometric or material constants (for example bubble size or surfactant properties, respectively) of the foam. Hence the need for modelling and simulation: developing a model which is able to correlate bulk rheological response, via parameters such as shear modulus and yield stress, with details of the microstructure of the foam and its surface chemistry is necessary before materials can be designed with particular properties.

Many theoretical and numerical predictions of foam response are available in the quasi-static limit of slow flows[14]. In contrast, Cantat[21] developed a non quasi-static two-dimensional model to predict the Herschel-Bulkley coefficients and showed how the yield stress increases with the shear rate due to bubble deformation. Nonetheless, her model neglects the curvature of films (each film is straight) and the concentration of surfactants at the interfaces is limited by a characteristic time for adsorption/desorption[21].

Here, we combine the Viscous Froth model[22] with a surfactant transfer model, as described in our previous publication[5], to analyse the rheological behaviour of dry two-dimensional foams. This model extends the two-dimensional Viscous Froth model[22], which includes the curvature of the films to simulate dry foams between parallel plates, by including the movement of surfactant molecules during foam flow[23]. As a consequence we are able to consider the tangential component of interface velocities which may be non-negligible at high deformation rate[24]. In addition to a characteristic time-scale relating to the external friction, the model has two free parameters related to the viscous and elastic properties of the interfaces.

We briefly review the model in section 2.1 and describe its numerical implementation for a disordered foam in section 2.2. The stress functional used in our simulations is described in section 2.3. We then investigate how the two free parameters associated with surfactant motion affect the stress response for two different protocols: simple shear strain (section 3), which gives information about the elastic shear modulus and the yield stress, and oscillatory strain (section 4), which gives the storage and loss modulus as a function of frequency or strain amplitude.

2 Viscous Froth Model with surfactant transport

2.1 Mathematical Model

The Viscous Froth model[22] describes the transport of curvature along the films of a two-dimensional dry foam[25]. The model extends the Young-Laplace law[4], observing that any imbalance between the film curvature K and the difference in gas pressure ΔP across the film is due to the dissipative friction between the films and the boundaries constraining the foam (see Figure 1). The dynamic equation for a single film with line tension γ and normal velocity v_n is

$$\lambda v_n = \Delta P - \gamma(\Gamma)K, \tag{1}$$

where λ is a drag coefficient. (We follow Kern *et al.*[22] and simplify the model by setting the exponent on the velocity, dictated by the details of the liquid flow in the Plateau borders between two bubbles and the boundary, to one.)

The intrinsic time scale of the model is $T_\lambda = \frac{\lambda L^2}{\gamma_{eq}}$, where L is a characteristic length of the model which we take to be the bubble size[5,22].

In contrast to the usual Viscous Froth model, we relax the assumption of constant surface tension γ (or more correctly a line tension) and allow it to be a function of the local concentration Γ of surfactant molecules on the film. We then apply the Langmuir equation of state, Eq.2, with Gibbs elasticity E, to calculate the local tension on each film:

$$\gamma = \gamma_{eq} - E \ln \frac{\Gamma}{\Gamma_{eq}}, \tag{2}$$

where γ_{eq} and Γ_{eq} are the equilibrium values of the surface tension and of the surfactant concentration respectively.

Knowing the surface tension gradient along each film, we define a "convection equation", similar to the Marangoni effect[26]. We assume that the gradient of surface tension is balanced by the drag experienced by the surfactant molecules which move along the film[5]. In this way our surfactant transport model allows the calculation of the tangential component of the surface velocity v_t in terms of a surfactant drag coefficient μ:

$$\mu v_t(s) - \frac{\partial \gamma}{\partial s} = 0, \tag{3}$$

where s is the curvilinear coordinate along the film.

From a dimensional analysis of equations 1, 2 and 3[5], we find the free parameters of the model: we define $\hat{E} = \frac{E}{\gamma_{eq}}$ and $\hat{\mu} = \frac{\mu}{\lambda}$. In our previous publication[5] we optimized $\hat{E}$ and $\hat{\mu}$ in order to fit ex-

perimental data and predict the Gibbs elasticity E and the surface viscosity μ for common anionic surfactants and dairy proteins. Experimental values for these physical parameters are available in literature, for the anionic surfactant SDS, for example, E is 30 mN/m while the surface viscosity μ is 1-10 mPa m s[5,27]. Varying the two free parameters in our model permits to investigate the effects of the elasticity and the surfactant drag on the behaviour of the foam.

With the exception of instantaneous topological changes, soap films meet in threes at the vertices of a dry foam. To model the dynamics of each vertex we extrapolate the assumptions in the viscous froth model to this situation: we balance the surface tension forces there, taking into account both the orientation and the tension of each of the three films (but not the pressures in the three bubbles), with the friction at the walls. Then the vertex velocity v_V is given by

$$\lambda \underline{v}_V + \frac{\sum \underline{\gamma}_i}{\sum l_i} = 0, \qquad (4)$$

where l_i is the length of the segment at the vertex, the vector $\underline{\gamma}_i = \frac{l_i}{|l_i|}\gamma_i$ with $i = 1,2,3$ and λ is the drag coefficient.

The model assumes a continuous exchange of surfactant molecules across vertices, as described by Satomi *et al.*[28], due to differences in the tension of the segments that meet there. We define the coefficient D_m to be the ratio between the concentration of surfactant at equilibrium and the surfactant drag coefficient μ times a reference length. The equation for the molecule movement is then

$$\frac{d(\Gamma_i l_i)}{dt} = D_m(\gamma_i - \gamma_k), \qquad (5)$$

where the label i takes the values, 1, 2 and 3 in turn while k takes the values 2, 3 and 1.

2.2 Numerical implementation
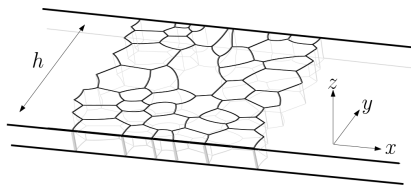
Fig. 1 Two-dimensional dry foam between two-plates.

We consider a single layer of bubbles between two flat plates as shown in Figure 1. The plates are flat and if the distance between them, in the z direction, is negligible in comparison to the bubble size, all the bubbles are prisms (with curved sides). Hence, the foam is identical at the contact with both plates and we can treat the system as two-dimensional[29].

To create a disordered foam of n bubbles with fully periodic boundary conditions (PBC) we start from the coordinates of n random seed points and generate a Voronoi tessellation.

We characterize the polydispersity of the foam by the second moment of the distribution of bubble areas, $\mu_2(A_b) = \frac{1}{n}\sum(A_b - A_{av})^2/A_{av}^2$, where A_{av} is the average area[30].

We ignore any inter-bubble gas diffusion (coarsening), which tends to occur on longer time-scales[6] than considered here. The foam is therefore effectively incompressible, bubble areas are constant, and we can apply the ideal gas law to calculate the pressure P_b in each bubble, as required in Eq. (1). For a bubble of area A_b we have $P_b A_b = C_w$ where C_w is a characteristic constant; we choose $C_w = 50$ which is large enough to keep the area fixed, *i.e.* the areas of each bubble at two successive time steps are accurate to within 10^{-8}. (Higher values of C_w do not affect the results but neither do they confer any advantage for the numerical method.) Note that the areas of the bubbles undergo a small initial variation as the foam evolves from the Voronoi tessellation towards an equilibrated configuration.

Starting from a given foam configuration, shown in Figure 2, each film is discretized into a number of short straight segments. We define two segments to meet at *points* within the film and three segments meet at a vertex. The lengths l of the segments are kept within tight bounds: $l_{min} = 0.021$ and $l_{max} = 0.12$. The lower bound also defines a minimum length l_{min} for topological rearrangements, or T1s: if the length of a segment connecting two vertices is shorter than l_{min} a T1, a microscopic plastic event, will be triggered, leading to a new foam configuration with lower energy and stress.

As explained above, the characteristic time for the viscous relaxation is $T_\lambda = \frac{\lambda L^2}{\gamma_{eq}}$, where we take $L = \sqrt{A_{av}}$ for the characteristic length-scale. Dimensional analysis of Eq.(3) leads to a similar definition of a characteristic time for surfactant transport: $T_\mu = \frac{\mu L^2}{\gamma_{eq}}$. We define a free parameter $\hat{\mu} = \frac{\mu}{\lambda}$ and as a consequence we can write $T_\mu = \hat{\mu}T_\lambda$. We assume that the surfactant drag is weaker than the friction with the walls, choosing for $\hat{\mu}$ a range of values between 0.1 and 1. The parameter $\hat{E}$ is derived from Eq.(2), which in dimensionless form can be written

$$\tilde{\gamma} = 1 - \hat{E}\ln\tilde{\Gamma}. \qquad (6)$$

We study the effect of the surface elasticity parameter for a range
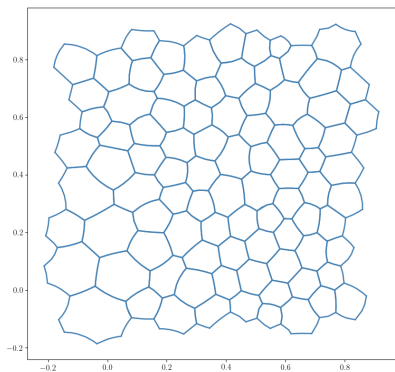
Fig. 2 Relaxed foam of $n = 100$ bubbles in the starting configuration that results from the equilibration of a Voronoi tesselation. The foam has periodic boundary conditions.

of values around one; with larger values of $\hat{E}$ the surface tensions acting at the vertices are weaker and therefore the films relax more slowly towards the final configuration of equilibrium[31]. On the contrary, values of $\hat{E}$ much lower than one, would render the variation of surface tension negligible.

The model is first applied to evolve the starting Voronoi configuration, with an initially uniform concentration of surfactant molecules and hence unit surface tension throughout the foam, towards an equilibrated foam. The velocities for each point are calculated as time derivatives of position with time-step $\delta t = 10^{-4}$. That is, at each step equations (1) and (3) are used to calculate the normal and tangential component of the velocity of each point along each film, while Eq. (4) is applied to move the vertices. In this way the structure evolves to satisfy Plateau's laws for a dry foam: all films have uniform curvature and meet in threes at angles of $120°$, as shown in Figure 2.

Once the foam has equilibrated, we apply a deformation and record the response. We consider two possible strain protocols, simple shear and oscillatory strain, in order to predict the rheological parameters of foams under different conditions.

To apply simple shear, we increase the horizontal coordinate of each point up to a strain of $\varepsilon = 5$. For a point on a film with position (x_t, y_t) at time t we determine its new position after an increment in the shear strain according to $x_{t+\Delta t} = x_t + \Delta t \dot{\varepsilon} y_t$ and $y_{t+\Delta t} = y_t$.

Following each increment in the applied strain we update the distribution of tension along each film through the Langumir Eq.(6) and we apply the VF and the ST Equations (1 and 3) to

relax the foam; we successively calculate the dynamics of the vertices and the displacement of surfactant molecules across adjacent films according to Equations (4) and (5). Note that the resulting structure is not an affine deformation of the initial configuration because of the viscous relaxation at each iteration.

For oscillatory strain we apply a sinusoidal strain of amplitude ε_0 and angular frequency ω, i.e. $\varepsilon = \varepsilon_0 \sin(\omega t)$. We describe the effect of varying the amplitude of the strain ε_0 or the frequency of oscillation ω in Sections 4.1 and 4.2 respectively, which requires that we first have an algorithm for calculating the relevant components of the stress tensor.

2.3 Calculation of the shear stress

The shear stress σ_{xy} gives qualitative and quantitative information about the rheological response of the foam. A linear relationship between stress and strain at small strains, for example, indicates elastic behaviour and allows the estimation of the elastic shear modulus G.

At higher strain the foam yields: this is a plastic response with many topological transformations as bubbles move past each other. The yield stress and yield strain are related through the elastic shear modulus.

Beyond the yield point the stress reaches a plateau, corresponding to a transition to liquid-like behaviour. The Bingham and (more often) Herschel-Bulkley models of yield stress fluids are often used to extract yield stress and shear-thinning information from the flow curve of a foam in this steady flow region[6].

However, as in many other "jammed" materials with a complex microstructure consisting of soft deformable objects[32], the plateau stress σ_Y is often lower than the stress σ_M at the yield point, a phenomenon known as a stress overshoot. As the foam is strained, it deforms elastically and stores elastic energy, until the σ_M is reached. Afterwards, the foam rearranges to a new configuration which is less deformed, thus relaxing stress[33]. The stress overshoot therefore depends on the orientation of the films and the elongation of the bubbles, which affect the transition of the foam from the solid-like to the liquid-like behaviour. In carbopol gels, Divoux *et al.*[1] highlighted that in the quasi-static regime, when $\dot{\varepsilon} < 10^{-3}$, this maximum shear stress is almost independent of strain-rate $\dot{\varepsilon}$, while at higher shear rates it increases as a weak power of the strain rate. For polymer solutions Ravindranath and Wang[34] found that σ_M varies linearly with the applied strain and they predicted that the strain at which the maximum stress is found varies as $\dot{\varepsilon}^{1/3}$.

For a foam, the maximum shear stress increases with the gas volume fraction, ϕ_g[35], and in the dry limit ($\phi_g \to 1$) this can be

captured with a tensorial model that accounts for rotation of the foam structure[32], at least in the quasi-static limit. The stress overshoot is even more pronounced at high shear rates[21].

Here the shear stress σ_{xy} is calculated using the formula derived by Batchelor[21,36]. This is a sum of the surface tension $\underline{\gamma}_i$ of each segment resolved in x and y directions over the whole foam. Since we are interested in the shear component of the stress tensor, the pressure contributions to the stress are not required. We determine the angle θ_i that each segment makes with the x axis, then

$$\sigma_{xy} = \frac{1}{nA_{av}} \sum_{\text{segments } i} \gamma_i \cos\theta_i \sin\theta_i \, l_i. \tag{7}$$

In the following we report the shear stress normalized by the Laplace pressure[7] $\hat{\sigma}_{xy} = \sigma_{xy}/(\gamma_{eq}/\sqrt{A_{av}})$.

3   Simple shear flow

3.1   Effect of shear rate on the shear stress

We consider a foam with $n = 320$ bubbles, average bubble area $A_{av} = 0.09$, and polydispersity $\mu_2(A_b) = 0.22$. We choose a range of values for the shear rate between 0.1 and 1; then the shear time-scale is in the range 1 to 10. The intrinsic time scale is $T_\lambda \approx 0.1$, so the relaxation within the foam is faster than the applied shear. Considering higher shear rates would lead to the opposite situation in which the shear drives the foam faster than it can relax, beyond the limits of our model.

Figure 3 shows the normalized shear stress calculated from Eq. (7), as a function of the strain, ε, at different shear rates, $\dot{\varepsilon}$.
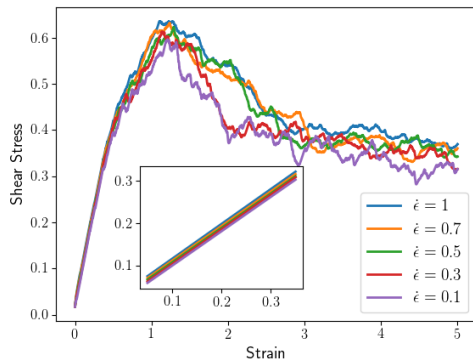
Fig. 3 Normalised shear stress versus strain for a dry foam subjected to simple shear at different shear rates $\dot{\varepsilon}$. The elastic and drag parameters are $\hat{E} = 1$ and $\hat{\mu} = 1$. The insert shows the stress-strain curves at small strains.

In the inset to Figure 3 we show that there are no plastic events

at small strains in the range $0.05 < \varepsilon < 0.35$ (in contrast to experiments on carbopol microgels[1]) and we therefore assume the foam to be purely elastic in the starting regime, allowing us to estimate the elastic shear modulus as a function of strain rate.

At higher deformations, the stress reaches a maximum value, σ_M, and then it slowly decreases towards a steady fluid-like response. As shown in Figure 3, σ fluctuates as the strain increases the foam flows[6]. The fluctuation in the shear stress is due to the presence of topological rearrangements, thus as long as the flowing foam changes its topology the stress never reaches a perfect plateau. We observe that the shear stress fluctuations increase at smaller shear rates. For these dry foams beyond the quasi-static regime, Figure 3 shows a slight increase of σ_M with increasing shear rate.

As we already observed yield stress and yield strain are related by the shear modulus, but a comprehensive knowledge of their relation with the overshot phenomenon is still missing. As usually happens in foam simulations, we observe the presence of few T1s before the maximum value σ_M is reached. In Section 4 we consider a foam with fewer bubbles and assume that the foam behaves as an elastic body for strains up to one so that we can fix $\varepsilon_0 = 1$ in order to investigate the effect of the angular frequency on the foam.

3.2   Effect of surfactant transport on the shear stress

Our model incorporates two parameters: one related to the interfacial elasticity ($\hat{E}$) and another to the drag on the surfactant molecules ($\hat{\mu}$) on each film. Here, we investigate the effect on the shear stress of two distinct contributions: the deformation of the bubbles, which changes the orientation of the films, and the surfactant motion along the film interfaces, which changes their surface tension.

In Figure 4 and 5 we plot the stress-strain curves obtained in the case of simple shear for different values of $\hat{\mu}$ and $\hat{E}$. For each simulation, we plot two curves: the stress-strain relationships calculated as if the tensions were constant (equal to the average tension γ_{av}), which represents the geometric contribution to the stress, plotted with dashed lines, and the shear stress obtained considering the actual surface tensions of the films.

Neglecting the variation of tension, the shear stress is determined by the film lengths and orientations. We would expect that in foams with greater elasticity the films are more stretched, increasing the shear stress. Comparing the dashed and solid lines in Figures 4 (a-c) indicates that, although we do not find a clear drop in the maximum shear stress with a decrease in the elastic parameter $\hat{E}$, the effect of the tensions is to increase the stress up

to yielding, and then to reduce it. The effect is partly explained by the average value of the tension which is $\gamma_{av} = 0.9151$. The gap widens (Figures 4(a-c)) as $\hat{E}$ increases, which in our model is related to the Gibbs elasticity, and hence the surface tension through Eq. (2).

In addition, changing $\hat{E}$ significantly modifies the structure of the foam and the distribution of T1 events, evident in the different shapes of the stress-strain curves in Figures 4(a-c). As the parameter $\hat{E}$ is reduced, the dynamics returns to the case of uniform tension.

The same behaviour is observed by decreasing the surfactant drag parameter $\hat{\mu}$: when $\hat{\mu} = 1.5$ the two curves for the shear stress are closer (Figure 5d), and so the effect of surface tension variations is small. Reducing $\hat{\mu}$, and therefore reducing the effect of drag on the surfactant molecules in the film, induces a larger gap between the lines (Figure 5f). Hence, the films evolve faster reaching smaller elongations, and as a consequence the concentration of molecules on films is higher and the tension drops through Eq. (2).

In the case of constant tension, weaker surfactant drag leads to films which are less elongated, and as a consequence the shear stress reported with dashed lines in figures 5(d-f) slightly decreases with $\hat{\mu}$. The variation of $\hat{\mu}$ significantly affects the shape of the stress-strain curves and therefore the distribution of the topological rearrangements in the foam.

Despite the small difference in magnitude between the dashed and the continuous lines in Figures 4 and 5, we show how the surface mechanical parameters, $\hat{E}$ and $\hat{\mu}$ affect the distribution of topological rearrangements and as a consequence, the foam configuration and the stress distribution across the foam.

3.3 Elastic Shear Modulus

From the shear stress data in Figure 3 we calculate the elastic shear modulus G' for different values of the shear rate $\dot{\varepsilon}$ between 0.1 and 1. That is, we calculate the slopes of the stress-strain curves at small deformations in the range $0.05 \leq \varepsilon \leq 0.35$. These are shown for various shear rates $\dot{\varepsilon}$ in Figure 6, either for fixed $\hat{\mu} = 1$ and varying $\hat{E}$, or *vice versa*.

We find that the elastic shear modulus slightly increases with higher values of shear rate. The slopes of the lines in Figure 6a are not significantly affected by the elastic parameter $\hat{E}$. For the surfactant drag coefficient $\hat{\mu}$, shown in Figure 6b, the slopes of the lines change with $\hat{\mu}$, suggesting that the effect of surfactant drag is more directly correlated to the shear rate. Our predictions agree qualitatively with experimental results in literature. Denkov *et al.*[37], for example, investigating foam rheology, found
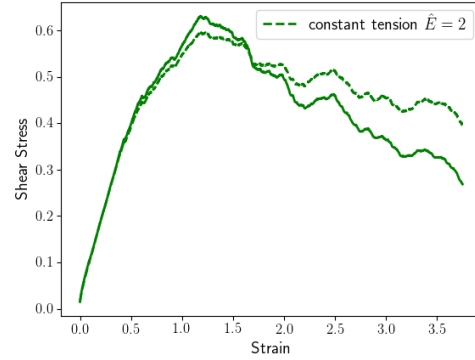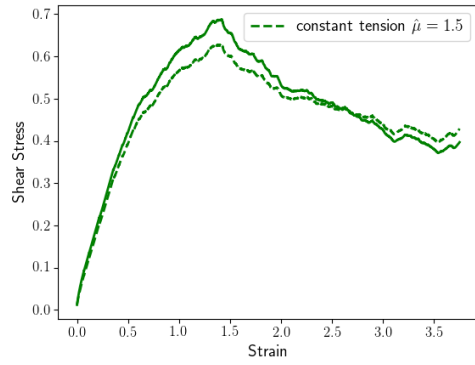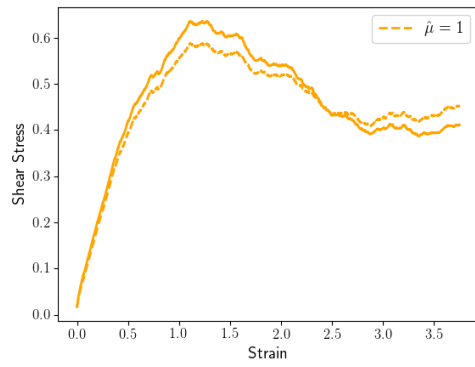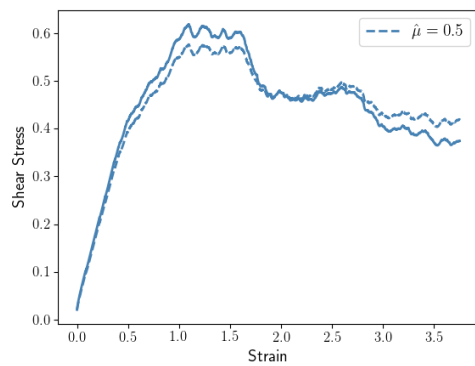

(a)
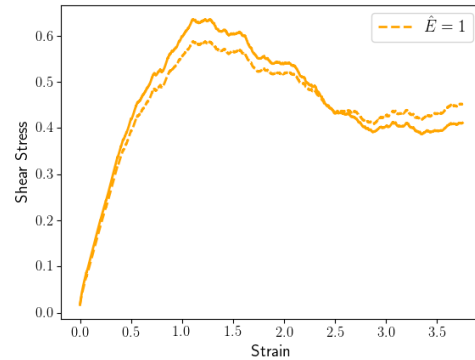
(b)
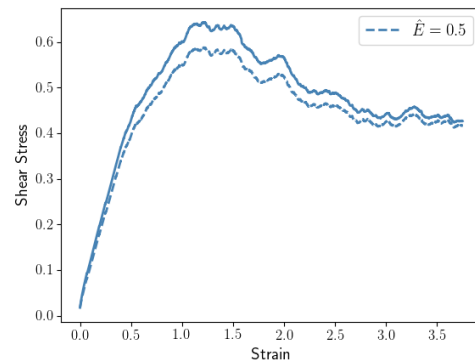
(c)

Fig. 4 Normalised shear stress versus strain for a dry foam subjected to steady shear with shear rate $\dot{\varepsilon} = 1$. The dashed lines indicate the value of stress that would be obtained if the surface tension were constant and equal to the average tension γ_{av}. a) b) c) Shear stress obtained for $\hat{\mu} = 1$ and varying $\hat{E}$ from 2 to 0.5. The plots show how greater elasticity and weaker surfactant drag act to reduce the shear stress in the foam.

(d)

(e)

(f)

Fig. 5 Normalised shear stress versus strain for a dry foam subjected to steady shear with shear rate $\dot{\varepsilon} = 1$. The dashed lines indicate the value of stress that would be obtained if the surface tension were constant and equal to the average tension γ_{av}. d) e) f) Shear stress calculated for $\hat{E} = 1$ and varying $\hat{\mu}$ from 1.5 to 0.5. The plots show how greater elasticity and weaker surfactant drag act to reduce the shear stress in the foam.
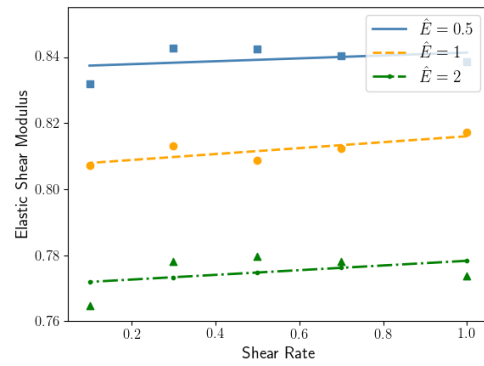
(a)
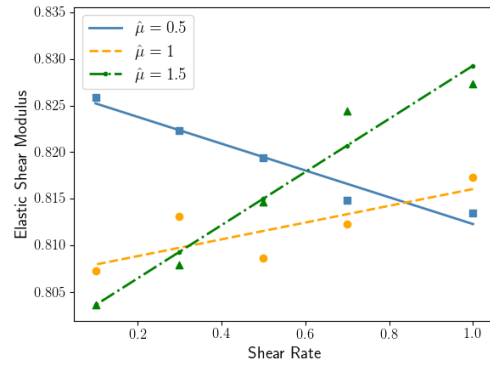
(b)

Fig. 6 Elastic shear modulus versus shear rate. We show straight-line fits through the data to guide the eye. (a) Surfactant drag parameter $\hat{\mu} = 1$ and varying $\hat{E}$. (b) Elastic parameter $\hat{E} = 1$ and varying $\hat{\mu}$.

that foams with high surface modulus surfactant, which are more viscous, relax slowly and are more dependent on the shear rate. Overall, the small changes in magnitude for the predicted values, suggest that the addition of the surfactant transfer leads to a higher order correction of the pre-existing VF model.

For a honeycomb foam consisting of hexagons with area A the shear modulus is $G' = \sqrt{\sqrt{3}/2}\ \gamma/\sqrt{A}$[12]. With the area A_{av}, the average tension γ_{av} and normalizing with the Laplace pressure we calculate $G' = 0.931$.

Cox and Whittick[12] showed that the shear modulus of a foam decreases with increasing disorder. For our disordered foam, with a polydispersity of 0.22, the shear modulus is therefore expected to be lower than for a honeycomb with the same average area; Figure 6 shows that this is the case.

Further, the shear modulus is higher if the interfaces are less elastic and the shear modulus increases more quickly at high shear rate if the interfaces impart more drag to the surfactant molecules.

3.4 Yield stress

Similarly to the shear modulus, the data in Figure 3 provides information about the yield stress σ_Y as a function of shear rate. Distinct from the maximum stress, σ_M, which corresponds to the overshoot in stress when the foam starts flowing, we take the yield stress to be the average of the stress at high strains that follows, *i.e.* the stress required to keep the foam flowing.

The shear stress is quite jagged (Figure 3), we calculate its mean and standard deviation for strains $\varepsilon > 3$, shown in Figure 7. The mean, and hence the yield stress, increases with increasing shear rate for all values of $\hat{E}$ and $\hat{\mu}$.

We find that the yield stress increases when the foam is less elastic and the surfactant drag effect more pronounced.

4 Oscillatory shear flow

4.1 Complex shear modulus as a function of frequency

We now consider a foam with $n = 100$ bubbles, average bubble area $A_{av} = 0.03$, and polydispersity $\mu_2(A_b) = 0.11$. We apply an oscillatory deformation $\varepsilon(t) = \varepsilon_0 \sin(\omega t)$ to the foam, where ε_0 is the maximum strain amplitude and ω the angular frequency. If the foam presents a linear viscoelastic behaviour, the corresponding stress is a sinusoidal function of amplitude σ_0 shifted by an angle δ, $\sigma(t) = \sigma_0 \sin(\omega t + \delta)$. We therefore write the stress in terms of two frequency dependent functions:

$$\sigma(t) = \varepsilon_0(G' \sin(\omega t) + G'' \cos(\omega t)). \tag{8}$$
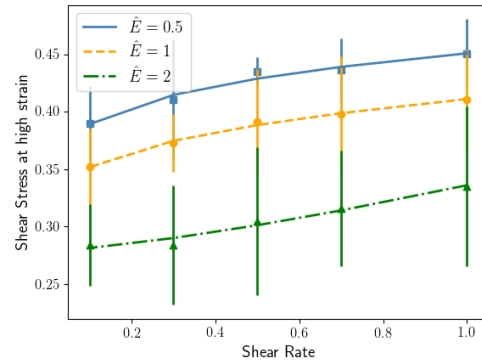

(a)
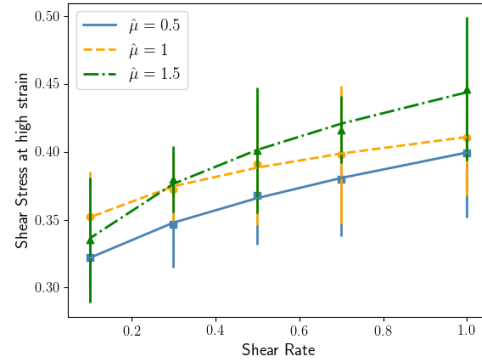
(b)

Fig. 7 Flow curves, that is, the mean value of the normalized shear stress, for $\varepsilon > 3$ versus shear rate $\dot{\varepsilon}$. (a) Varying elastic parameter $\hat{E}$ with surfactant drag parameter $\hat{\mu} = 1$. (b) Varying $\hat{\mu}$ with $\hat{E} = 1$.

Materials with high shear modulus are highly rigid, while fluids have a shear modulus of zero, therefore any force deforms its surface. Foams are complex fluids, they present small shear modulus and the application of a shear strain leads to plastic deformations, as we have discussed in Section 3. Starting from Eq.8 we calculate the two components of the shear modulus, G' and G'', defining the storage and loss moduli as

$$G' = \frac{\sigma_0}{\varepsilon_0} \sin(\delta), \; G'' = \frac{\sigma_0}{\varepsilon_0} \cos(\delta). \qquad (9)$$

The storage modulus, G', represents the elastic energy stored in the material, while the loss modulus, G'', takes into account the viscous dissipation. Starting from a disordered foam at equilibrium we apply an oscillatory deformation and we calculate the corresponding shear stress via Eq. (7). Fitting the resulting shear stress profile to a sinusoidal function we find the unknown variables σ_0 and δ, and deduce the shear moduli through Equations (9).

We analyse the shear modulus for a disordered foam subjected to oscillatory strain at a range of frequencies. In Figure 8 we report the normalized shear stress as a function of strain, varying the frequency of oscillation between 0.1 and 10, with fixed amplitude, $\varepsilon_0 = 1$, below the yield strain (cf Figure 10, where for amplitudes above 1 the hysteresis cycle is no longer elliptical).
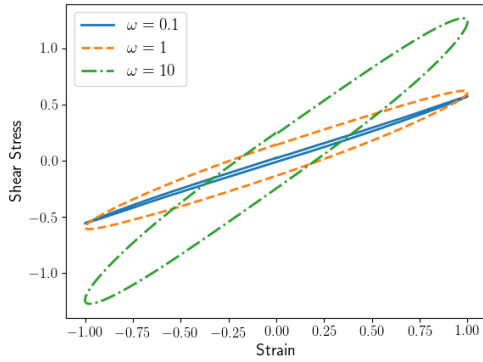

Fig. 8 Normalized shear stress versus strain in oscillatory shear with three values of frequency ω and amplitude $\varepsilon_0 = 1$. The elastic and drag parameters are $\hat{E} = 1$ and $\hat{\mu} = 1$.

The stress-strain graph (Figure 8) exhibits an elliptic shape which confirms that the foam behaves like a viscoelastic material at such a strain amplitude and tells us that the dissipation in the foam is predominantly of viscous (rather than plastic) origin. As a consequence, it is straightforward to fit the shear stress with

a sinusoidal function and calculate the storage and loss moduli through Eqs. 9.
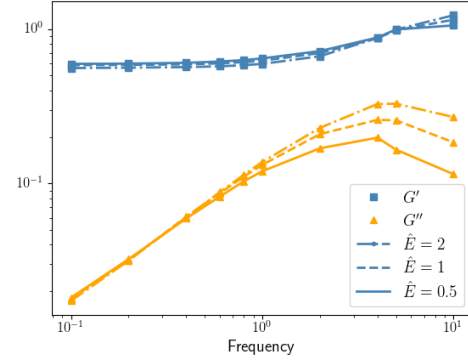
(a)
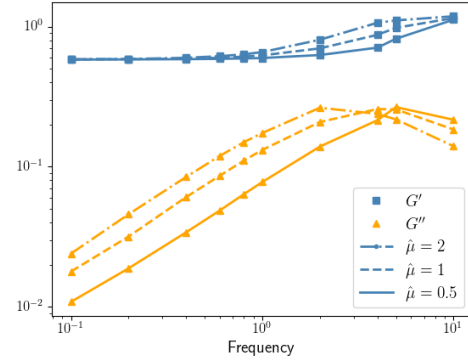
(b)

Fig. 9 Complex shear moduli versus frequency with strain amplitude $\varepsilon_0 = 1$. (a) Varying elastic parameter $\hat{E}$ with surfactant drag parameter $\hat{\mu} = 1$. (b) Varying $\hat{\mu}$ with $\hat{E} = 1$.

Figure 9 shows the storage and loss modulus as a function of frequency. These results agree qualitatively with the measurements reported in literature[6,38,39]. We found that the storage modulus is higher than the loss modulus, as what usually happens for materials with a solid-like behaviour[2]. The loss modulus presents a higher dependence on the frequency; G'' increases at higher frequency when the foam is flowing faster, causing the increment of viscous dissipation. Increasing the elastic parameter $\hat{E}$ has a negligible effect on the storage modulus G' but increases the loss modulus at high frequencies. Conversely, increasing the surfactant drag $\hat{\mu}$ shifts the small rise in the storage modulus G'

and the peak in the loss modulus G'' to lower frequencies.

## 4.2 Complex shear modulus as a function of strain amplitude

We now focus on the nonlinear viscous, elastic and plastic response of a two-dimensional foam when the applied strain is large enough to induce a transition from solid-like to liquid-like behaviour. In Section 4.1 we measured the visco-elastic behaviour of the foam by applying an oscillatory strain at an amplitude just below the yield strain. We now increase the amplitude beyond the yield strain.

In this case it is no longer possible to approximate the shear stress as a sinusoid; instead, for larger strain amplitudes a strong strain hardening is observed at each strain cycle, which leads to non-negligible non-linearity in the stress. This transition from linear to nonlinear response is due to plastic events, i.e. irreversible bubble rearrangements or T1s.

We apply a periodic oscillatory shear and record, in Figure 10a, the normalized shear stress for different maximum strain amplitudes, ε_0. We report only the stresses related to the second period of oscillation (Figure 10b), for which it is evident that increasing ε_0 above the yield strain leads to a transition of the shape of the hysteresis cycle from an ellipse to a parallelogram, in agreement with theoretical and experimental results [16,18]. This tells us that the dissipation in the foam has no longer only a viscous origin but also a plastic one.

In Figure 11 we report the components of the complex shear modulus versus the strain amplitude. The complex shear modulus is calculated starting from the decomposition of the stress in a Fourier series, as reported in the literature [16,17]. In agreement with the experimental results of Labiausse *et al.*[40], we find that up to a strain of amplitude 0.1, G' and G'' do not present any strong evolution with the strain amplitude.

Close to the yield strain we find that the storage modulus G' starts to drop, thus the foam stops deforming elastically and it loses elastic energy. The foam starts flowing causing the increment of viscous dissipation[6] as indicated by the G'', which increases leading to a cross-over between G' and G''. In agreement with experimental data[40], we find that the cross-over occurs when the strain amplitude is close to one. At higher strain amplitudes, the loss moduli becomes higher than the storage moduli which then confirms the transition of the foam behaviour to liquid-like.. Finally, at high amplitude both the storage and the loss modulus decrease. There is a strong dependence of the loss modulus on the surfactant drag parameter at small amplitude, as shown in Figure 9(b), confirming the data in Figure 11(b). Costa
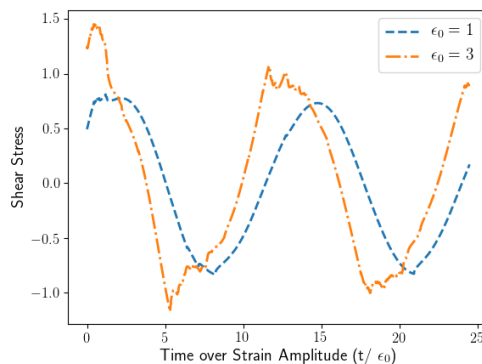

(a)
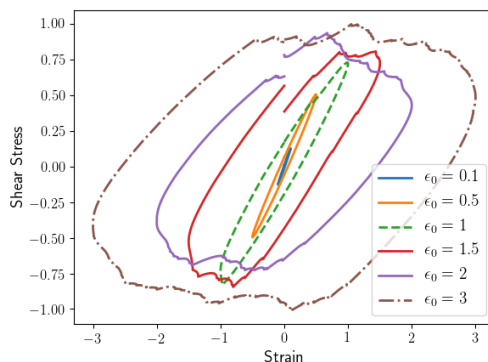
(b)

**Fig. 10** (a) Normalized shear stress versus scaled time for two different values of the maximum strain amplitude, with unit frequency of oscillation. The elastic and drag parameters are $\hat{E} = 1$ and $\hat{\mu} = 1$ respectively. Time is scaled by the strain amplitude so that the curves roughly coincide. (b) Hysteresis cycles related to the second period of oscillation, for different strain amplitudes ε_0.
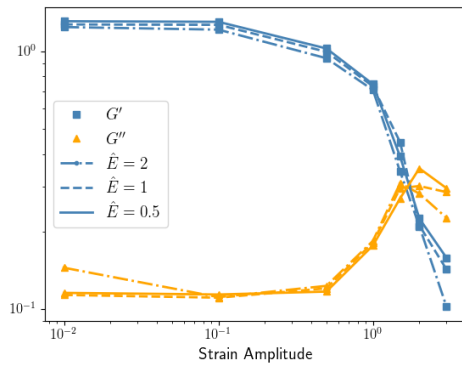
(a)
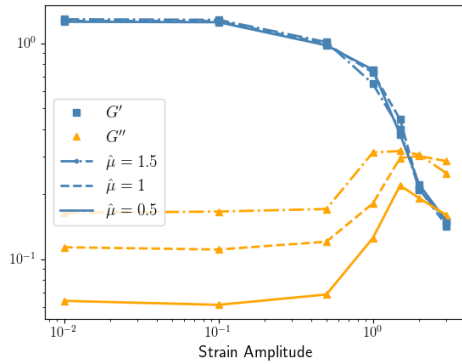
(b)

Fig. 11 Storage and loss modulus versus strain amplitude with frequency $\omega = 1$, shown on logarithmic axes. (a) Varying elastic parameter $\hat{E}$ with surfactant drag parameter $\hat{\mu} = 1$. (b) Varying $\hat{\mu}$ with $\hat{E} = 1$.

et al.[41] carried out experiments to measure the complex shear modulus as a function of liquid viscosity, and our predictions of the variation of the loss modulus with the superficial viscosity agree with the experimental observations.

5   Conclusions

We have incorporated a model for surfactant transport in the viscous froth model to simulate a flowing two-dimensional dry foam in which the motion of the foam is affected by friction with the walls of the container and where the surfactant is tracked as it moves along and between the soap films. Following equilibration of the foam a simple shear strain or an oscillating strain is applied to the foam, allowing us to predict the rheological parameters of a foam in which such effects are important.

The first question to address is therefore how the variation of surface tension affects the stress response of the foam. We find that either increasing the elastic parameter or decreasing the surfactant drag causes the shear stress to drop at higher strains.

Furthermore the stress-strain curves give us qualitative and quantitative information about the foam properties and their dependence on the rate of application of the strain. At small strain we predict the elastic shear modulus G' and find that with higher surfactant drag G' becomes more dependent on shear rate.

Overall we demonstrate how our model can be used as a tool to predict characteristic rheological parameters such as the elastic shear modulus, the yield stress, and the complex shear modulus.

We find that smaller interfacial elasticity leads to a higher drop in the loss modulus, a drop which increases at higher frequencies of oscillation. Decreasing the surfactant drag shifts the loss modulus to lower frequencies. Increasing the amplitude of the applied strain instead leads to irreversible plastic deformations. The elasticity at the interface has little effect on the shear modulus while decreasing the surfactant drag leads to lower energy losses (decreasing loss modulus).

Having investigated the effect on the surfactant transport on the macroscopic behaviour of the foam, the model should now be extended to wet foams in which the thickness of the films and the disjoining pressure within them are non-negligible.

Acknowledgements

Notes and references

1 T. Divoux, C. Barentin and S. Manneville, *Soft Matter*, 2011, **7**, 9335–9349.

2 R. G. Larson, *The Structure and Rheology of Complex Fluids*, Oxford University Press: New York, 1999.

3 D. Carugo, D. N. Ankrett, X. Zhao, X. Zhang, M. Hill, V. O'Byrne, J. Hoad, M. Arif, D. D. Wright and A. L. Lewis, *Phlebology*, 2016, **31**, 283–295.

4 D. Weaire and S. Hutzler, *The physics of foams*, Oxford University Press, 2001.

5 F. Zaccagnino, A. Audebert and S. J. Cox, *Phys. Rev. E*, 2018, **98**, 022801.

6 I. Cantat, S. Cohen-Addad, F. Elias, F. Graner, R. Höhler, O. Pitois, F. Rouyer and A. Saint-Jalmes, *Foams: structure and dynamics*, OUP Oxford, 2013.

7 H. Princen, *Journal of Colloid and interface science*, 1983, **91**, 160–175.

8 N. P. Kruyt, *J. Appl. Mech.*, 2007, **74**, 560–567.

9 D. Stamenović, *Journal of Colloid and Interface Science*, 1991, **145**, 255–259.

10 K. A. Brakke, *Experimental mathematics*, 1992, **1**, 141–165.

11 A. M. Kraynik and D. A. Reinelt, *Journal of Colloid and interface Science*, 1996, **181**, 511–520.

12 S. J. Cox and E. L. Whittick, *The European Physical Journal E*, 2006, **21**, 49–56.

13 A. M. Kraynik, D. A. Reinelt and F. van Swol, *Physical Review Letters*, 2004, **93**, 208301.

14 R. Höhler and S. Cohen-Addad, *Journal of Physics: Condensed Matter*, 2005, **17**, R1041.

15 L. Bressy, P. Hebraud, V. Schmitt and J. Bibette, *Langmuir*, 2003, **19**, 598–604.

16 P. Marmottant and F. Graner, *Soft Matter*, 2013, **9**, 9602–9607.

17 P. Marmottant and F. Graner, *The European Physical Journal E*, 2007, **23**, 337–347.

18 F. Rouyer, S. Cohen-Addad, R. Höhler, P. Sollich and S. Fielding, *The European Physical Journal E*, 2008, **27**, 309–321.

19 P. Coussot, D. Laigle, M. Arattano, A. Deganutti and L. Marchi, *Journal of hydraulic engineering*, 1998, **124**, 865–868.

20 G. Ovarlez, S. Rodts, A. Ragouilliaux, P. Coussot, J. Goyon and A. Colin, *Physical Review E*, 2008, **78**, 036307.

21 I. Cantat, *Soft Matter*, 2011, **7**, 448–455.

22 N. Kern, D. Weaire, A. Martin, S. Hutzler and S. Cox, *Physical Review E*, 2004, **70**, 041411.

23 P. Grassia, C. Oguey and R. Satomi, *The European Physical Journal E*, 2012, **35**, 64.

24 A. Bussonnière, E. Shabalina, X. Ah-Thon, M. L. Fur and I. Cantat, *arXiv preprint arXiv:1902.07076*, 2019.

25 R. Satomi, P. Grassia, S. Cox, G. Mishuris and L. Lue, *Proceedings of the Royal Society A: Mathematical, Physical and Engineering Sciences*, 2013, **469**, 20130359.

26 D. A. Edwards, H. Brenner and D. T. Wasan, *Interfacial transport processes and rheology*, Boston, 1991.

27 M. Durand and H. A. Stone, *Physical review letters*, 2006, **97**, 226101.

28 R. Satomi, P. Grassia and C. Oguey, *Colloids and Surfaces A: Physicochemical and Engineering Aspects*, 2013, **438**, 77–84.

29 W. Drenckhan, S. J. Cox, G. Delaney, H. Holste, D. Weaire and N. Kern, *Colloids and Surfaces A: Physicochemical and Engineering Aspects*, 2005, **263**, 52–64.

30 A. Wyn, I. T. Davies and S. J. Cox, *The European Physical Journal E*, 2008, **26**, 81–89.

31 F. Zaccagnino, *PhD thesis*, Department of Mathematics, Aberystwyth University, 2019.

32 C. Raufaste, S. J. Cox, P. Marmottant and F. Graner, *Physical Review E*, 2010, **81**, 031404.

33 P. Sollich, F. Lequeux, P. Hébraud and M. E. Cates, *Physical review letters*, 1997, **78**, 2020.

34 S. Ravindranath and S.-Q. Wang, *Journal of Rheology*, 2008, **52**, 681–695.

35 S. A. Khan, C. A. Schnepper and R. C. Armstrong, *Journal of Rheology*, 1988, **32**, 69–92.

36 G. K. Batchelor, *An introduction to fluid dynamics*, Cambridge university press, 1967.

37 N. D. Denkov, S. Tcholakova, K. Golemanov, K. Ananthpadmanabhan and A. Lips, *Soft Matter*, 2009, **5**, 3389–3408.

38 S. Cohen-Addad, H. Hoballah and R. Höhler, *Physical Review E*, 1998, **57**, 6897.

39 A. Gopal and D. J. Durian, *Physical review letters*, 2003, **91**, 188303.

40 V. Labiausse, R. Höhler and S. Cohen-Addad, *Journal of Rheology*, 2007, **51**, 479–492.

41 S. Costa, R. Höhler and S. Cohen-Addad, *Soft Matter*, 2013, **9**, 1100–1112.